Measurement report: Crustal materials play an increasing role in elevating particle pH: Insights from 12-year records in a typical inland city of China.

Hongyu Zhang[1,2], Shenbo Wang [2,3]*, Zhangsen Dong [1,2]*, Xiao Li [2,3], Ruiqin Zhang[2,3]

[1] College of Chemistry, Zhengzhou University, Zhengzhou, 450000, China

[2] Research Institute of Environmental Sciences, Zhengzhou University, Zhengzhou 450000, China

[3] School of Ecology and Environment, Zhengzhou University, Zhengzhou, 450000, China

* Corresponding authors: Shenbo Wang and Zhangsen Dong

E-mail address: shbwang@zzu.edu.cn and dzszzu1990@163.com

Abstract

Particle acidity serves as a key determinant in atmospheric chemical processes. Emerging concerns regarding aerosol acidity trends have been highlighted amid China's sustained initiatives to mitigate emissions of both acidic and alkaline precursors, especially in North China, which is significantly affected by dust aerosol. 12-year observational data in Zhengzhou reveal that the annual average $PM_{2.5}$ concentration decreased from 162 ± 81 μg/m^3 in 2011 to 60 ± 41 μg/m^3 in 2022, with the largest reduction in sulfate (73%). Correspondingly, the annual particle pH increased by 0.10 units from 2011 to 2019. In addition, the elevated particle pH in 2015 and 2018 was notably influenced by the increase in TNH_x ($NH_3 + NH_4^+$). Note that the crustal material concentrations and their proportions increased significantly during 2019–2022, which might be responsible for the resuspension of surrounding soil dust. Even though the TNH_x concentration was decreasing, the annual average growth rate of pH values increased to 0.21 units from 2019 to 2022. This phenomenon is not unique to Zhengzhou, as major cities in the North China Plain have also experienced a pronounced upward trend in coarse particles after 2019. Therefore, the long-term evolution of particle acidity in North China will require comprehensive consideration of synergistic effects involving acidic precursors, ammonia, and crustal materials.

Keywords: Dust, aerosol acidity, sources, North China Plain, control measurement

Synopsis: The future ammonia reduction policies in North China may not lead to a rapid increase in particle acidity in the presence of crustal materials., which further elevated the particle pH after 2019.

Graphical abstract:
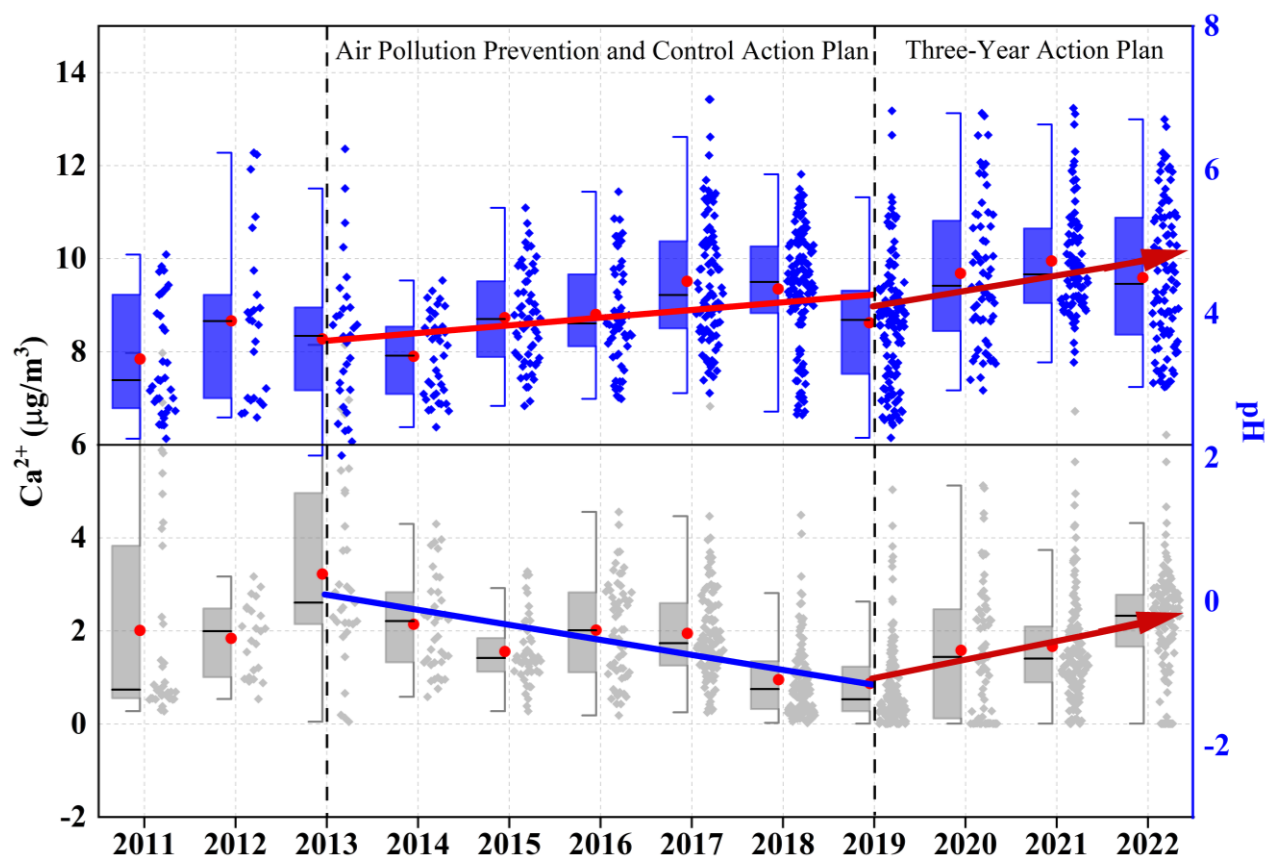
Highlights:

• Crustal material concentrations and their proportions increased significantly during 2019–2022;

• The resuspension of surrounding soil dust may determine the rebound of crustal material

concentrations;

• Rebound in crustal material further elevated the particle pH.

1 Introduction

Particle acidity is a critical parameter that affects atmospheric chemistry, such as the gas-particle partitioning of semi-volatile and volatile species (Surratt et al., 2010; Guo et al., 2016), the solubility of metals (Tao and Murphy, 2019), acid-catalyzed reactions (Rengarajan et al., 2011), and acid deposition (Mao et al., 2009), thereby determining aerosol concentration and chemical composition, as well as impacting human health, ecosystems, and climate (Li et al., 2017; Pye et al., 2020; Su et al., 2020; Nenes et al., 2021). Generally, the global fine particulate matter (PM$_{2.5}$, aerodynamic diameter ≤ 2.5 μm) exhibits a bimodal pH distribution ranging from 1–3 (e.g., in the United States and Europe) (Guo et al., 2015; Battaglia et al., 2017; Masiol et al., 2020; Zhang et al., 2021) and 4–5 (e.g., in East Asia) (Kim et al., 2022; Sharma et al., 2022). The atmosphere rich in gaseous ammonia (NH$_3$) and crustal material (CM) shows significant pH buffering effects (Wang et al., 2020; Zheng et al., 2020; Karydis et al., 2021), which is a dominant factor that drives the high particle pH in East Asia (Karydis et al., 2021; Zhang et al., 2021; Kim et al., 2022; Sharma et al., 2022).

In recent years, the changing trends in particle pH have become a research focus, especially in China, in response to air pollution control policies, i.e., Air Pollution Prevention and Control Action Plan (2013–2018) and Three-Year Action Plan (2018–2020). The annual average PM$_{2.5}$ concentration in Beijing dropped by 64% from 89.5 μg/m³ in 2013 to 32 μg/m³ in 2023 (MEP, 2023), with a clear downward trend of sulfate concentration, and nitrate surpassing sulfate as the primary component (Zhai et al., 2019; Zhou et al., 2019; Li et al., 2023). The atmospheric behavior of ammonium, governed by gas-particle partitioning processes involving ammonia (NH$_3$) as the predominant alkaline gas,

demonstrates notable stability in concentration levels, with observational records showing less than 5%

interannual variation in NH_3 column densities over North China during 2015–2019 (Dong et al., 2023).

Under such conditions, the dominant inorganic aerosol component transitions from ammonium sulfate

to ammonium nitrate. This compositional shift enhances atmospheric particulate hygroscopicity due

to ammonium nitrate's superior water uptake capability, ultimately elevating particle pH levels through

aqueous-phase dilution mechanisms (Wexler and Seinfeld, 1991; Pinder et al., 2007, 2008; Heald et

al., 2012; Weber et al., 2016). For instance, a significant increase in the nitrate-to-sulfate molar ratio

from 2014–2017 in Beijing resulted in the particle pH increasing from 4.4 to 5.4 (Xie et al., 2020).

Moreover, increased NH_3 concentrations raised particle pH by 0.3–0.4 units from 2014/2015 to

2018/2019 in Beijing (Song et al., 2019). Over Europe and North America, the pH has increased

strongly from about 2.8 and 2.2 during the 1970s to 3.9 and 3.3 in 2020 respectively, especially during

the 1990s, with significantly increasing NH_3 emission (Karydis et al., 2021). On the contrary, modeling

results indicate a continuous decline in pH in East Asia from 1970 to 2020 due to sharp increases in

SO_2 and NO_x emissions (Karydis et al., 2021). In addition, the $PM_{2.5}$ pH showed a slight decrease of

0.13 from 2018 to 2022 summer in Beijing due to the change in total nitrate (NO_3^- + HNO_3) (Li et al.,

2023). Moreover, Zhou et al. (2022) found a decreasing pH trend from 2011 to 2019 in eastern China,

primarily influenced by temperature, followed by sulfate and non-volatile cations. Similarly, Nah et al.

(2023) observed a decreasing pH trend from 2011 to 2020 in Hong Kong, attributing it to temperature

and sulfate levels. Thus, concerns have been raised about the potential increase in the acidity of aerosol

and precipitation due to China's ongoing efforts to reduce ammonia emissions, which pose severe

health risks and acid deposition (Liu et al., 2019; Shi al., 2019).

85   In addition to NH$_3$, CM is another key alkaline substance that buffers particle pH. Ca^{2+} can form

86   insoluble CaSO$_4$ with sulfate, reducing sulfate concentration in the aqueous phase of aerosol, and thus

87   lowering H$^+$ and aerosol liquid water content (ALWC) concentrations and enhancing particle pH (Ding

88   et al., 2019; Karydis et al., 2021). Moreover, non-volatile cations can lower the molar ratio of ammonia

89   to sulfate, leading to an increase in particle pH (Zheng et al., 2022). Karydis et al. (2021) framework

90   demonstrated that CM played a critical buffering role in sustaining aerosol pH around 7 across the

91   Middle East arid regions. The model sensitivity tests revealed that under hypothetical dust-free

92   conditions (CM = 0), aerosol acidity would escalate to pH~4 due to NH$_4^+$/SO$_4^{2-}$ domination. Wang et

93   al. (2022) reported that non-volatile cations accounted for approximately 8–17% of hourly aerosol pH

94   variation. Li et al. (2023) indicated that the buffering effect of cations was the major reason for the

95   relatively small pH changes from 2018 to 2022 in Beijing, emphasizing that reducing coarse particle

96   emissions in the future could significantly decrease particle pH. In addition, there was a rising trend in

97   the contribution of CM to particle pH in Tianjin, China (Shi et al., 2017). Therefore, it is evident that

98   CM has a significant impact on the variation of particle pH, especially in North China, which is

99   significantly affected by dust aerosol, but the trend of CM concentration and its long-term implications

100   is still lacking unfortunately.

101   Zhengzhou presents unique atmospheric chemistry that distinguishes it from other mega-cities in

102   North China. As the capital of China's foremost agricultural province (Henan Province, contributing

103   18% of national NH$_3$ emissions), Zhengzhou's PM$_{2.5}$ composition combined substantial crustal

104   material (15 ± 3% in PM$_{2.5}$ vs. <10% in Beijing) with exceptional ammonia abundance (Huang et al.,

105   2012; Liu et al., 2018; Wang et al., 2018). This created distinct particle acidity characteristics,

106　maintaining pH 4.5–6.0 compared to lower pH levels (3.3–5.4) in other cities like Beijing (Ding et

107　al.,2019; Zhang et al., 2021). However, two critical research gaps persist: (1) the long-term evolution

108　of CM under control policies remains unquantified; (2) the role of CM on pH buffer capacity in NH_3-

109　enriched environments lacks systematic assessment.

110　　To address these gaps, our study pioneers the first multi-decadal analysis (2011–2022) coupling

111　$PM_{2.5}$ components with thermodynamic modeling through three key innovations: (1) revealing the

112　long-term trends of CM, (2) analyzing the variations of CM sources, and (3) exploring pH trend and

113　its relationship with CM. The resultant findings advance our understanding of urban aerosol acidity

114　chemistry by underscoring the critical role of CM.

2 Experiment and method

2.1 Instruments and Measurements

117　　Sampling was conducted on the fourth-floor platform at Zhengzhou University (34.75° N, 113.61°

118　E) in Zhengzhou, China. The sampling site (Fig. S1), approximately 14 m above the ground, is

119　primarily surrounded by residential areas with well-developed transportation networks and no

120　significant industrial sources. There are two highways located 3 km to the south and 7 km to the east.

121　Additionally, a coal-fired power plant located 6 km to the east was shut down in 2020, and a gas-fired

122　power plant is situated 3 km to the south.

123　　Samples were collected using a high-volume sampler (TE-6070D, Tisch, USA) and air particulate

124　samplers (TH-16A, Tianhong, China) from April 2011 to December 2022. Two quartz filters and two

125   Teflon filters were used daily from 10:00 AM to 9:00 AM the next day, resulting in a total of 5848

126   samples. After excluding abnormal data due to instrument malfunctions, 4228 valid samples were

127   obtained. Detailed information on the samples is provided in Table S1. Organic carbon (OC) and

128   elemental carbon (EC) were analyzed using a carbon analyzer (Model 5L, Sunset Laboratory, USA).

129   Water-soluble inorganic ions (Cl^-, NO_3^-, SO_4^{2-}, Na^+, NH_4^+, K^+, Mg^{2+}, and Ca^{2+}) were measured using

130   ion chromatography (ICS-90 and ICS-900 models, Dionex, USA) (Yu et al., 2017; Jiang et al., 2018).

131   Elements were analyzed using a wavelength dispersive X-ray fluorescence spectrometer (S8 TIGER,

132   Bruker, Germany) to determine concentrations of Fe, Na, Mg, Al, Si, Cl, K, Ca, V, Ni, Cu, Zn, Cr, Mn,

133   Co, Cd, Ga, As, Se, Sr, Sn, Sb, Ba, and Pb (Tremper et al., 2018). Meteorological conditions, including

134   temperature (T), relative humidity (RH), and wind speed (WS) were obtained using an automatic

135   weather station (Wang et al., 2019). Blank filters were also routinely analyzed with each batch of

136   samples to detect sample contamination and provide quality assurance on the elemental concentrations.

137   Detailed analytical methods and quality control are described in the supplement (Text S1). The method

138   detection limits and measurement uncertainties are summarized in Table S2. The quality assurance

139   protocol excluded temporally discrete dust storm and precipitation periods to prevent contamination

140   of the source analysis of CM and modeling particle pH, given that such events induce non-

141   representative extremes in both crustal element concentrations and pH values, coupled with elevated

142   PM measurement uncertainties. The annual mean $PM_{2.5}$ concentration data for cities in the North China

143   Plain were obtained from the China National Environmental Monitoring Center (CNEMC), available

144   at https://www.cnemc.cn/.

2.2 Data Analysis

2.2.1 Mass reconstruction

The calculation method for CM is as follows (Tian et al., 2016):

$$[CM]=1.89\times[Al] + 2.14\times[Si] + 1.4\times[Ca] + 1.43\times[Fe]+1.94[Ti] \tag{1}$$

where [Al], [Si], [Ca], [Fe] and [Ti] represent the concentrations of the respective elements ($\mu g/m^3$), but Ti was not measured.

2.2.2 Thermodynamic model

The particle pH was calculated using the ISORROPIA-II mode (version 2.1, http://isorropia.eas.gatech.edu). The input data (excluding RH ≤ 30%), including SO_4^{2-}, TNO_3 (HNO_3 + NO_3^-), TNH_x (NH_3+ NH_4^+), Ca^{2+}, K^+, Na^+, Mg^{2+}, Cl^-, RH and T, with the temporal resolution aligned with the sampling periods (from 10:00 AM to 9:00 AM the following day). The concentrations of hydrogen ions in air (H_{air}^+) and ALWC were derived from the Na^+-K^+-Ca^{2+}-Mg^{2+}-NH_4^+-SO_4^{2-}-NO_3^--Cl^--H_2O equilibrium composition system. Activity coefficients for H^+ and OH^- were fixed at unity, while other ion pairs (e.g., H^+-Cl^-) employed the Kusik-Meissner parameterization for ionic activity calculations (Fountoukis and Nenes, 2007). pH values were calculated using the following formula:

$$pH = -\log_{10}H_{aq}^+ \cong -\log_{10}\frac{1000H_{air}^+}{ALWC_i + ALWC_o} \cong -\log_{10}\frac{1000H_{air}^+}{ALWC_i} \tag{2}$$

$$ALWC_o = \frac{m_{org}\rho_w}{\rho_w}\frac{\kappa_{org}}{\left(\dfrac{1}{RH}-1\right)} \tag{3}$$

where $ALWC_i$ and $ALWC_o$ refer to the ALWC for inorganic and organic components, respectively.

9

163 m_{org} denotes the mass of organic aerosol, ρ_w is the density of water (1.0 g/cm^3), ρ_{org} is the density of

164 organic material (1.4 g/cm^3) (Guo et al., 2015), k_{org} is the hygroscopicity parameter for organic aerosol

165 (0.087) (Chang et al., 2010; Li et al., 2016). The ISORROPIA-II model operated under metastable

166 conditions in the forward mode. Due to the lack of measured data for gaseous HNO$_3$ and NH$_3$, TNO$_3$

167 was represented solely by NO$_3^-$. The concentration of NH$_3$ was simulated based on a linear regression

168 equation proposed by Wei et al. (2023), who used the same data as this study from 2013 to 2020:

169 $$NH_3 = 19.909 \times RH + 0.559 \times T - 0.35 \times NH_4^+ + 0.123 \times NO_3^- + 2.159 \times Cl^- - 0.224 \times SO_4^{2-} - 154.923 \quad (4)$$

170 where NO$_3^-$, SO$_4^{2-}$, NH$_4^+$, and Cl$^-$ correspond to their respective concentrations (μg/m^3). To validate the

171 applicability of Equation 4 for annual NH$_3$ estimation and pH simulation in Zhengzhou, this study

172 utilized both observed NH$_3$ data (from a Thermo Scientific URG-9000D ambient ion monitor, USA)

173 and calculated NH$_3$ values derived from Equation 4 at the same monitoring site throughout 2022,

174 inputting them into the thermodynamic model for pH simulation. As shown in Figure S2, pH values

175 calculated from observed and simulated NH$_3$ exhibit good agreement ($r = 0.97$, $P < 0.01$). Furthermore,

176 NH$_3$ concentrations modeled by ISORROPIA demonstrate a significant correlation ($r = 0.95$, $P < 0.01$)

177 with that simulated NH$_3$ by Equation 4. These results collectively demonstrate the reliability of the

178 NH$_3$ estimation method in this study.

179 **2.2.3 HYSPLIT analysis**

180 Backward trajectories were calculated using the mixed-particle Lagrangian integrated trajectory

181 method (HYSPLIT, https:// www.ready.noaa.gov/HYSPLIT_traj.php). Meteorological input data were

182 from the Global Data Assimilation System (GDAS) with 3D wind vectors, temperature, relative

183 humidity, geopotential height, surface pressure, and boundary layer diagnostics. 24-hour backward

184 trajectories were simulated for air masses arriving at 100 m above ground level in Zhengzhou, a

185 receptor height aligned with the city's average elevation (~100 m above sea level) to capture near-

186 surface pollutant transport dynamics within the boundary layer.

187 Trajectories from 2013–2018 and 2019–2022 were independently clustered via the Angle Distance

188 algorithm to compare policy-driven variations (Wang et al., 2009). The optimal cluster number (three,

189 Figure S3) was determined by tracking total spatial variance (TSV), with classification finalized at the

190 inflection point preceding the second TSV surge.

191 3 Results and discussion

192 3.1 Temporal variations in chemical components

193 Over the past twelve years, the Chinese government has implemented two major policies to

194 mitigate air pollution: the Air Pollution Prevention and Control Action Plans (2013–2018) and the

195 Three-Year Action Plan (2018–2020), with key targets and measures detailed in Tables S3 and S4. The

196 2013–2018 policy prioritized end-of-pipe controls in power generation and heavy industries,

197 mandating $\geq$10% PM_{10} reduction nationwide and region-specific $PM_{2.5}$ reduction targets (25% for

198 Beijing-Tianjin-Hebei, 20% for Yangtze River Delta, and 15% for Pearl River Delta). Subsequently,

199 the 2018–2020 campaign shifted toward structural reforms and multi-pollutant synergistic governance,

200 enforcing $\geq$15% nationwide SO_2/NO_x emission cuts and $\geq$18% $PM_{2.5}$ reduction in non-compliant cities

201 relative to 2015 levels.

202   The long-term trends in PM$_{2.5}$ concentrations and its chemical components in Zhengzhou from

203   2011 to 2022 are depicted in Fig. 1, with annual average concentrations listed in Table 1.

204   Correspondingly, the annual average concentration of PM$_{2.5}$ in Zhengzhou decreased from 162 ± 81

205   μg/m^3 in 2011 to 60 ± 41 μg/m^3 in 2022, representing a reduction of approximately 63%. In particular,

206   the reduction rate reached 72% after 2013. As for chemical components, the largest reductions were

207   observed in SO$_4^{2-}$ (79%), decreasing from 38.0 ± 19.9 μg/m^3 in 2013 to 7.9 ± 4.5 μg/m^3 in 2022,

208   followed by EC (76%). Additionally, the concentrations of NH$_4^+$ and NO$_3^-$ also significantly decreased

209   by 68% and 56%, respectively. The proportion of each component in PM$_{2.5}$ (Fig. S4) reveals a decrease

210   in SO$_4^{2-}$, K$^+$, and Cl$^-$, indicating effective control measures targeting coal and biomass combustion (Lei

211   et al., 2021). However, the proportions of NO$_3^-$ and OC in PM$_{2.5}$ rose from 11% and 12% in 2013 to

212   13% and 17% in 2022, respectively, similar to the trend observed in the North China Plain (Wen et al.,

213   2018; Zhai et al., 2019; Li et al., 2023).

214   **3.2 Temporal variations in CM**

215   Notably, there is no clear declining trend in the CM concentration, with a rebound observed during

216   2020–2022 (Fig. 1i). Furthermore, the proportion of CM in PM$_{2.5}$ exhibits a significant upward trend

217   (Fig. S4). To further analyze its trend, sampling data were divided into three periods corresponding to

218   governmental stages: 2011–2013, when no special control measures were implemented; 2013–2019,

219   coinciding with the implementation of the Air Pollution Prevention and Control Action Plan; and

220   2019–2022, coinciding with the Three-Year Action Plan. During these periods, Henan Province and

221   Zhengzhou City implemented several dust control policies summarized in Table S5. As shown in Fig.

222   2a and 2b, the mass concentration of CM peaked at 14.6 ± 8.3 μg/m^3 in 2013, accounting for 8% of

223   PM$_{2.5}$. To evaluate the inter - annual change trend of CM, the Mann - Kendall method, Sen's slope,

224   and Least - Squares (LS) slope were comprehensively used with the results presented in Table S6.

225   From 2013 to 2019, the CM concentration notably decreased from 14.6 ± 8.3 to 8.5 ± 7.8 μg/m^3, with

226   an annual average decline rate of 0.81 μg/(m^3·year) from LS slope [0.015 μg/(m^3·year) from Sen's

227   slope]. Apart from control measures, the interannual meteorological analysis shows (Fig. S5) WS

228   exhibited a declining trend, with a decrease rate of 43%, while RH showed an increasing trend at a rate

229   of 8% from 2013 to 2019, under which conditions that were unfavorable for dust resuspension (Wang

230   et al., 2013, 2018). Seasonal trends (Fig. S6) reveal significant declines in CM during spring in 2013–

231   2019 with WS decreasing from 2.2 m/s in 2013 to 1.4 m/s in 2019 (Fig. S7) and stable RH (Fig. S8).

232   Similarly, summer CM reductions in 2013–2019 corresponded with WS declines. These patterns

233   suggest spring-summer CM improvements resulted from the synergistic effects of meteorological

234   changes and dust control policies. Conversely, autumn-winter seasons showed limited CM reductions

235   despite comparable WS decreases in 2013–2019, highlighting the need for enhanced dust emission

236   controls in Zhengzhou during these seasons. As for the individual crustal elements in Fig. S9, Ca

237   exhibited the highest average annual decline rate of 33% during 2013–2019, followed by Al. Si showed

238   a less pronounced decline, attributed to its association with soil dust, where control measures for

239   exposed soil are lacking (Zhang et al., 2020). In addition, the Ca^{2+} concentration as depicted in Fig. 2c

240   decreased from 3.2 ± 2.1 μg/m^3 in 2013 to 2.2 ± 1.1 μg/m^3 in 2019, with an approximate annual average

241   decline rate of 0.32 μg/(m^3·year) from LS slope [4.14E–03 μg/(m^3·year) from Sen's slope] in Table

242   S6, further demonstrating the decline in dust source. It was worth noting that the proportions of CM,

243 Ca, Al, Fe, Si, and Ca^{2+} in $PM_{2.5}$ have shown consecutive annual increases from 2013 to 2019, with

244 CM proportion increasing from 8% in 2013 to 14% in 2019, indicating that CM reduction lagged

245 behind $PM_{2.5}$ reduction efforts in Zhengzhou during this period. Additionally, both concentration and

246 proportion of Ca^{2+} in 2022 (2.2 ± 1.1 μg/m^3 and 5%) were higher than in other cities of China, such as

247 Beijing (1.0 μg/m^3 and 2.8%), Tianjin (0.5 μg/m^3 and 1.4%), and Xiamen (0.48 μg/m^3 and 1.5%) (Shi

248 et al., 2017; Xu et al., 2025; Zhang et al., 2021). These results indicate that CM remained an important

249 component of $PM_{2.5}$ in Zhengzhou City.

250 During 2019–2022, both CM and Ca^{2+} concentrations exhibited significant rebounds, with annual

251 growth rates of 0.24 and 0.4 μg/(m^3·year) from LS slope [5.80E–03 and 5.42E–03 μg/(m^3·year) from

252 Sen's slope], respectively, and their proportions increased from 14% and 2% in 2019 to 22% and 5%

253 in 2022. CM concentrations rebounded in all seasons, particularly in winter (Fig. S6). Changes in

254 meteorological conditions may be a significant factor contributing to these concentration rebounds,

255 accompanied by the average WS increased by 0.14 m/s and RH decreased by 7% from 2020 to 2022

256 (Fig. S5, S7, and S8), facilitating dust resuspension. Furthermore, the lack of more effective dust

257 control measures, as indicated by the absence of significant changes in the dust control policies from

258 the Air Pollution Prevention and Control Action Plan and Three-Year Action Plan, may be another

259 important factor contributing to the rebound of dust.

260 **3.3 Sources of CM**

261 Elemental ratios were employed to characterize the sources of CM, with the Ca/Al ratio widely

262 recognized as a reliable indicator of sandy origin (Zhang et al., 2017). In addition, significant variations

263   in Ca/Si ratios (Table S7) were observed among different dust sources (Road, Construction, Piles, Soil).

264   Fig. 3a illustrates the trend in Ca/Si ratios from 2011 to 2022. After 2013, Ca/Si ratios showed a

265   declining trend annually, with the average ratio decreasing from a peak of 1.6 in 2016 to a lowest of

266   0.4 in 2022. Compared with Ca/Si ratios from different types of dust sources, the effect of road and

267   construction dust on CM has gradually decreased. This may be attributed to the implementation of dust

268   control measures such as enclosure, shielding, and dust suppression at construction and demolition

269   sites, as well as dust control on ground surfaces and roads (Table S5). During 2019–2022, the average

270   Ca/Si ratio remained below 1, with a mean of 0.4 in 2022, indicating that soil dust predominantly

271   contributed to CM. Currently, measures for controlling soil-suspended dust are limited, primarily

272   relying on long-term strategies such as afforestation and increasing urban green coverage, thus

273   requiring a longer process and sustained investment.

274   Sand dust transport serves as a significant source of CM in the North China Plain (Zhang et al.,

275   2024). The Ca/Al ratio from 2016 to 2022 (Fig. 3b) shows minimal variation, with annual averages

276   ranging between 1.5 and 2.5, indicating no significant changes in the source regions of sand. The

277   transport trajectories (Fig. 3c and 3d) reveal that a marked decline in the contribution of long-distance

278   sand dust transport originating from Inner Mongolia (via Shaanxi and Shanxi provinces) from 13.9%

279   during 2013–2018 to 7.2% in 2019–2022. In contrast, local transport within Henan province and short-

280   distance transport from Shandong province exhibited contrasting increases. These findings suggest

281   that the rebound in CM concentrations during 2019–2022 in Zhengzhou might be responsible for the

282   resuspension of surrounding soil dust.

3.4 Long-term trend of particle pH

284   Are shown in Fig. 4 and Table S6, pH values showed a clearly increasing trend after 2014. From

285   2013 to 2019, the annual pH increased by 0.11 units from the LS slope [9.15E–04 units from Sen's

286   slope], reaching a maximum median value of 4.45 (Mean: 4.35) in 2018. Note that the annual average

287   growth rate of pH values increased to 0.21 units from LS slope [2.93E–03 units from Sen's slope] from

288   2019 to 2022, with a maximum median value of 4.42 (Mean: 4.51) in 2022. Seasonally, pH values

289   showed increasing trends in spring, summer, and autumn, and notably increased in winter from 2020

290   to 2022 (Fig. S10). The increasing trend in pH values observed in this study is similar to the findings

291   in Beijing (Song et al., 2019; Xie et al., 2020), presumably attributable to the comparable chemical

292   composition trends and meteorological conditions (Liu et al., 2017; Wang et al., 2020; Xu et al., 2015).

293   In contrast, Shanghai and Hong Kong display divergent trends (Nah et al., 2023; Zhou et al., 2022).

294   This disparity might be ascribed to the stronger buffering effect exerted by NH_3 and dust in Zhengzhou

295   than marine aerosols (Na^+/Cl^-) in these coastal cities (Shi et al., 2017; Liu et al., 2019). Moreover,

296   these coastal cities' warm climates amplify pH declines. Elevated temperatures reduce ALWC through

297   moisture evaporation, concentrating H^+ and directly lowering pH. Concurrently, heat-enhanced NH_3

298   volatilization from particulate NH_4^+ weakened acid neutralization (Zhou et al., 2022; Nah et al., 2023).

299   Sensitivity analyses were conducted to explore the dominant factors driving the elevated particle

300   pH in Zhengzhou by giving a range for one parameter (i.e., TNH_x) and average values for other

301   parameters (i.e., SO_4^{2-}, NO_3^-, Na^+, Cl^-, Ca^{2+}, K^+, Mg^{2+}, RH, and T) input into the ISORROPIA-II model.

302 Are shown in Fig. S11, particle pH increases with the cation concentrations (e.g., TNH_x, K^+, Ca^{2+},

303 Mg^{2+}, and Na^+) and decreases with anion concentrations (e.g., SO_4^{2-} and NO_3^-). Additionally, RH does

304 not significantly affect pH, whereas an increase in T leads to a noticeable decrease in particle pH.

305   Based on the sensitivity analysis curves, the pH values corresponding to a variable in different

306 years were calculated according to the average values of this variable in different years (Table S8).

307 The difference in pH values of this variable between two adjacent years was defined as ΔpH which is

308 illustrated in Fig. 5. According to Equation (2), in addition to H^+ concentration, particle pH is primarily

309 influenced by the dilution effect of ALWC. Moreover, ALWC affects the gas-particle partitioning of

310 semi-volatile compounds, thereby influencing particle acidity (Zuend et al., 2010; Zuend and Seinfeld,

311 2012). As shown in Fig.5 and Table S8, only in 2015, 2019, and 2020 did the increases in ALWC

312 concentration (17.6 μg/m³, 4.1 μg/m³, and 11.6 μg/m³, respectively) lead to pH increases of 0.22, 0.06,

313 and 0.14 units. This clearly cannot fully explain the significant pH increase in Zhengzhou since 2013.

314 Notably, since 2013, H^+ concentration has shown a decreasing trend. Particularly, H^+ concentrations

315 decreased by 7.6×10^{-6}, 11.2×10^{-6}, and 7.2×10^{-6} mol/L in 2013, 2015, and 2017, respectively,

316 leading to pH increases of 0.21, 0.36, and 0.42 units. After 2019, a continuous decline in H^+

317 concentration was observed for three consecutive years, resulting in pH increases of 0.21, 0.13, and

318 0.2 units in 2020, 2021, and 2022, respectively. These findings indicate that the increase in pH from

319 2019 to 2022 in Zhengzhou was primarily driven by the reduction in H^+ concentration.

320   The concentration of H^+ in the aerosol liquid phase is influenced by both chemical composition

321 and meteorological conditions. To further understand the factors affecting ΔpH, we analyzed the

322 variations in $PM_{2.5}$ chemical components and meteorological parameters. Results indicate that the

323   decline in SO_4^{2-} from 2013 to 2018 was the primary cause of the increase in particle pH, as it decreased

324   H^+ and ALWC concentrations (Fig. S12) in aerosol (Ding et al., 2019; Zhang et al., 2021). The average

325   SO_4^{2-} concentration decreased by 14.6 and 5.3 $\mu g/m^3$, resulting in a pH increase of 0.43 and 0.35 units

326   from 2013 to 2014 and 2016 to 2017, respectively, which was comparable to an increased rate of 0.3

327   units in East Asia due to SO_2 emission controls since 2016 (Karydis et al., 2021). As another acidic

328   ion, the decrease in nitrate concentration did not significantly contribute to the pH increases, consistent

329   with findings from Ding et al. (2019) and Zhang et al. (2021). This is primarily because NO_3^- declined

330   more slowly compared to sulfate ions and exceeded sulfate concentrations after 2016, under which

331   conditions that nitrate-rich particles can absorb twice the amount of water that sulfate-rich particles,

332   leading to an increase in ALWC concentration and inhibiting pH decline (Lin et al., 2020; Xie et al.,

333   2020). On the other hand, increases in particle pH in 2015 and 2018 were notably influenced by

334   changes in TNH_x with concentrations increased by 5.5 and 1.3 $\mu g/m^3$, respectively. Increased TNH_x

335   concentrations could react with SO_4^{2-} or NO_3^- and consume a substantial amount of H^+, thereby raising

336   particulate matter pH values (Seinfeld et al., 1998; Zhang et al., 2021). Substantial decreases in T in

337   2015 (4.2°C), 2017 (4.9°C), and 2018 (2.8°C), favoring NH_3 partitioning into the particle phase and

338   reducing H^+ concentrations, drove increases in particle pH (Tao and Murphy, 2019).

339   During the period from 2020 to 2022, the influence of SO_4^{2-} on particle pH gradually decreased,

340   with a decrease in concentration from 0.3 to 2.3 $\mu g/m^3$ (Table S8) only bringing about a pH decrease

341   of 0.03 to 0.14 (Fig. 5). Moreover, a rebound in SO_4^{2-} concentration to 7.9 ± 4.5 $\mu g/m^3$ in 2022 even

342   resulted in a decrease of 0.11 units in pH instead. On the other hand, TNHx began to show a slight

343   annual decline (0.9 to 2.2 $\mu g/m^3$), resulting in a significant decrease in pH (0.21–0.35). Consequently,

344 the increase in pH values was closely related to the rise in Ca^{2+} concentration. Ca^{2+} is less volatile and

345 competes preferentially with NH_3 to neutralize anions such as SO_4^{2-} to form insoluble $CaSO_4$, which

346 precipitates from the aerosol aqueous phase (Ding et al., 2019; Karydis et al., 2021), thereby reducing

347 H^+ concentrations (Fig. S12) and subsequently lowering particle acidity. Specifically, increases of 0.7

348 and 0.5 μg/m^3 in Ca^{2+} concentrations led to pH increases of 0.13 and 0.09 units in 2020 and 2022,

349 respectively, making Ca^{2+} a primary controlling factor for pH elevation.

4 Conclusions

351   The annual average PM$_{2.5}$ concentration in Zhengzhou decreased from 212.4 ± 101.5 μg/m^3 in

352 2013 to 59.5 ± 41.2 μg/m^3 in 2022, with the largest reduction in SO_4^{2-}. As for CM, their concentrations

353 notably decreased from 2013 to 2019, because of effective dust control measures, as well as decreased

354 wind speed and increased relative humidity. However, the proportions of CM in PM$_{2.5}$ have shown

355 consecutive annual increases. In addition, CM concentrations and their proportions increased

356 significantly during 2019–2022, which might be responsible for the resuspension of surrounding soil

357 dust. Correspondingly, the annual pH increased by 0.11 units from 2013 to 2019 mainly due to the

358 decline in SO_4^{2-}, increased TNH$_x$, or decreased temperature. During the period from 2020 to 2022, the

359 annual average growth rate of pH values increased to 0.21 units from 2019 to 2022, which was

360 determined by the rise in Ca^{2+} concentration.

5 Implication

Control measures implemented by the Chinese government have proven effective in reducing dust, but this study reveals that the crustal materials in $PM_{2.5}$ rebounded after 2019. This phenomenon is not unique to Zhengzhou, as major cities in the North China Plain have also experienced a pronounced upward trend in coarse particles after 2019 (Fig. S13). Thus, crustal materials persist as a substantial constituent of atmospheric aerosols in North China, sustaining elevated particle pH levels. Extensive research has established that heightened particle pH inhibits nitrate reduction in aerosols (Ding et al., 2019; Lin et al., 2020; Wen et al., 2018), particularly significant given nitrate's predominant role in haze formation within this region. Notably, while moderately acidic aerosols demonstrate reduced health impacts, particles with pH < 3 exhibit substantially greater health risks (Shi et al., 2019). Consequently, future environmental management strategies must prioritize real-time assessment of regulatory impacts on particle acidity. This necessitates an integrated approach that simultaneously addresses acidic precursors, alkaline precursors, and crustal material contributions to atmospheric acid chemistry.

Data availability

All the data presented in this article can be accessed through https://doi.org/10.5281/zenodo.14032007 (Zhang, 2024).

Supporting Information

Additional data, figures, and tables, some of which are referenced directly within the manuscript, and detailed descriptions of field measurements and samples.

Author contributions

S.W. designed this study. H.Z. and Z.D. analyzed the data and prepared the manuscript with the contributions of all coauthors. X.L. conducted measurements. R.Z. provided funding acquisition. All authors have read and agreed to the published version of the manuscript.

Competing interests

The authors declare that they have no conflict of interest.

Acknowledgment

Funding Sources

References

Battaglia, M. A.; Douglas, S.; Hennigan, C.: Effect of the urban heat island on aerosol pH, Environ. Sci. Technol., 51, 13095–13103, https://doi.org/10.1021/acs.est.7b02786, 2017.

Chang, R. Y. W.; Slowik, J. G.; Shantz, N. C.; Vlasenko, A.; Liggio, J.; Sjostedt, S. J.; Leaitch, W. R.; Abbatt, J. P. D. The hygroscopicity parameter (κ) of ambient organic aerosol at a field site subject to biogenic and anthropogenic influences: relationship to degree of aerosol oxidation. Atmos. Chem. Phys., 10, 5047–5064, https://doi.org/10.5194/acp-10-5047-2010, 2010.

Ding, J., Zhao, P., Su, J., Dong, Q., Du, X., and Zhang, Y.: Aerosol pH and its driving factors in Beijing, Atmos. Chem. Phys., 19, 7939–7954, https://doi.org/10.5194/acp-19-7939-2019, 2019.

Dong, J., Li, B., Li, Y., Zhou, R., Gan, C., Zhao, Y., Liu, R., Yang, Y., Wang, T., and Liao, H.: Atmospheric ammonia in China: Long-term spatiotemporal variation, urban-rural gradient, and influencing factors, Sci. Total Environ., 883, 163733, https://doi.org/10.1016/j.scitotenv.2023.163733, 2023.

Fountoukis, C and Nenes, A.: ISORROPIA II: a computationally efficient thermodynamic equilibrium model for K^+ - Ca^{2+} - Mg^{2+} - NH_4^+ - Na^+ - SO_4^{2-} - NO_3^- - Cl^- - H_2O aerosols, Atmos. Chem. Phys., 7, 4639–4659, https://doi.org/10.5194/acp-7-4639-2007, 2007.

Guo, H., Sullivan, A. P., Campuzano-Jost, P., Schroder, J. C., Lopez-Hilfiker, F. D., Dibb, J. E., Jimenez, J. L., Thornton, J. A., Brown, S. S., Nenes, A., and Weber, R. J.: Fine particle pH and the

22

partitioning of nitric acid during winter in the northeastern United States, J. Geophys. Res. Atmos., 121, 10,355–310,376, https://doi.org/10.1002/2016JD025311, 2016.

Guo, H., Xu, L., Bougiatioti, A., Cerully, K. M., Capps, S. L., Hite Jr, J. R., Carlton, A. G., Lee, S. H., Bergin, M. H., Ng, N. L., Nenes, A., and Weber, R. J.: Fine-particle water and pH in the southeastern United States, Atmos. Chem. Phys., 15, 5211–5228, https://doi.org/10.5194/acp-15-5211-2015, 2015.

Heald, C.; Collett, J. J.; Lee, T.; Benedict, K.; Schwandner, F.; Li, Y.; Clarisse, L.; Hurtmans, D. R.; Van, D. M.; Clerbaux, C.; Coheur, P. F., Philip, S.; Martin, R. V.; Pye, T.: Atmospheric ammonia and particulate inorganic nitrogen over the United States, Atmos. Chem. Phys., 12, 10295–10312, https://doi.org/10.5194/acp-12-10295-2012, 2012.

Huang, X., Song, Y., Li, M., Li, J., Huo, Q., Cai, X., Zhu, T., Hu, M., and Zhang, H.: A high-resolution ammonia emission inventory in China, Global. Biogeochem. Cy., 26, GB1030, https://doi.org/10.1029/2011GB004161, 2012.

Jiang, N.; Duan, S.; Yu, X.; Zhang, R.; Wang, K. Comparative major components and health risks of toxic elements and polycyclic aromatic hydrocarbons of $PM_{2.5}$ in winter and summer in Zhengzhou: Based on three-year data. Atmos. Res., 213, 173–184, https://doi.org/10.1016/j.atmosres.2018.06.008, 2018.

Karydis, V. A., Tsimpidi, A. P., Pozzer, A., and Lelieveld, J.: How alkaline compounds control atmospheric aerosol particle acidity, Atmos. Chem. Phys., 21, 14983–15001, https://doi.org/10.5194/acp-21-14983-2021, 2021.

Kim, Y., Park, O., Park, S. H., Kim, M. J., Kim, J.-J., Choi, J.-Y., Lee, D., Cho, S., and Shim, S.: $PM_{2.5}$ pH estimation in Seoul during the KORUS-AQ campaign using different thermodynamic models, Atmos. Environ., 268, 118787, https://doi.org/10.1016/j.atmosenv.2021.118787, 2022.

Lei, L., Zhou, W., Chen, C., He, Y., Li, Z., Sun, J., Tang, X., Fu, P., Wang, Z., and Sun, Y.: Long-term characterization of aerosol chemistry in cold season from 2013 to 2020 in Beijing, China, Environ. Pollut., 268, 115952, https://doi.org/10.1016/j.envpol.2020.115952, 2021.

Li, C.; Hu, Y.; Chen, J.; Ma, Z.; Ye, X.; Yang, X.; Wang, L.; Wang, X.; Mellouki, A. Physiochemical

properties of carbonaceous aerosol from agricultural residue burning: Density, volatility, and hygroscopicity. Atmos. Environ., 140, 94–105, https://doi.org/10.1016/j.atmosenv.2016.05.052, 2016.

Li, W., Xu, L., Liu, X., Zhang, J., Lin, Y., Yao, X., Gao, H., Zhang, D., Chen, J., Wang, W., Harrison, R. M., Zhang, X., Shao, L., Fu, P., Nenes, A., and Shi, Z.: Air pollution-aerosol interactions produce more bioavailable iron for ocean ecosystems, Sci. Adv., 3, e1601749, https://doi.org/10.1126/sciadv.1601749, 2017.

Li, Y., Lei, L., Sun, J., Gao, Y., Wang, P., Wang, S., Zhang, Z., Du, A., Li, Z., Wang, Z., Kim, J. Y., Kim, H., Zhang, H., and Sun, Y.: Significant reductions in secondary aerosols after the Three-Year Action Plan in Beijing summer, Environ. Sci. Technol., 57, 15945–15955, https://doi.org/10.1021/acs.est.3c02417, 2023.

Lin, Y., Zhang, Y., Fan, M, and Bao, M.: Heterogeneous formation of particulate nitrate under ammonium-rich regimes during the high-$PM_{2.5}$ events in Nanjing, China, Atmos. Chem. Phys., 20, 3999–4011, https://doi.org/10.5194/acp-20-3999-2020, 2020.

Liu, M.; Huang, X.; Song, Y.; Tang, J.; Cao, J.; Zhang, X.; Zhang, Q.; Wang, S.; Xu, T.; Kang, L.; Gai, X.; Zhang, H.; Yang, F.; Wang, H.; Yu, J.; Lau, A.; He, L.; Huang, X.; Duan, L.; Ding, A.; Xue, L.; Gao, J.; Liu, B.; Zhu, T. Ammonia emission control in China would mitigate haze pollution and nitrogen deposition, but worsen acid rain. Proc. Natl. Acad. Sci., 116, 7760–7765, https://doi.org/10.1073/pnas.1814880116, 2019.

Liu, M., Song, Y., Zhou, T., Xu, Z., Yan, C., Zheng, M., Wu, Z., Hu, M., Wu, Y., and Zhu, T.: Fine particle pH during severe haze episodes in northern China, Geophys. Res. Lett., 44, 5213–5221, https://doi.org/10.1002/2017GL073210, 2017.

Liu, Z., Gao, W., Yu, Y., Hu, B., Xin, J., Sun, Y., Wang, L., Wang, G., Bi, X., Zhang, G., Xu, H., Cong, Z., He, J., Xu, J., and Wang, Y.: Characteristics of $PM_{2.5}$ mass concentrations and chemical species in urban and background areas of China: emerging results from the CARE-China network, Atmos. Chem. Phys., 18, 8849-8871, https://doi.org/10.5194/acp-18-8849-2018, 2018.

Mao, I., Lin, C., Lin, C., Chen, Y., Sung, F., and Chen, M.: Exposure of acid aerosol for

469   schoolchildren in metropolitan Taipei, Atmos. Environ., 43, 5622–5629, https://doi.org/10.

470   1016/j.atmosenv.2009.07.054, 2009.

471 Masiol, M., Squizzato, S., Formenton, G., Khan, M. B., Hopke, P. K., Nenes, A., Pandis, S. N., Tositti,

472   L., Benetello, F., Visin, F., and Pavoni, B.: Hybrid multiple-site mass closure and source

473   apportionment of $PM_{2.5}$ and aerosol acidity at major cities in the Po Valley, Sci. Total Environ.,

474   704, 135287, https://doi.org/10.1016/j.scitotenv.2019.135287, 2020.

475 MEP (Ministry of Environment Protection), 2023. https://www.mee.gov.cn/ywdt/hjywnews/2024

476   06/t20240605_1075031.shtml, Accessed date:5 June 2024.

477 Nah, T., Lam, Y. H., Yang, J., and Yang, L.: Long-term trends and sensitivities of $PM_{2.5}$ pH and aerosol

478   liquid water to chemical composition changes and meteorological parameters in Hong Kong,

479   South China: Insights from 10-year records from three urban sites, Atmos. Environ., 302,

480   https://doi.org/10.1016/j.atmosenv.2023.119725, 2023.

481 Nenes, A., Pandis, S. N., Kanakidou, M., Russell, A. G., Song, S., Vasilakos, P., and Weber, R. J.:

482   Aerosol acidity and liquid water content regulate the dry deposition of inorganic reactive nitrogen,

483   Atmos. Chem. Phys., 21, 6023–6033, https://doi.org/10.5194/acp-21-6023-2021, 2021.

484 Pinder, R., Adams, P., and Pandis, S.: Ammonia emission controls as a cost-effective strategy for

485   reducing atmospheric particulate matter in the eastern United States, Environ. Sci. Technol., 41,

486   380–386, https://doi.org/10.1021/es060379a, 2007.

487 Pinder, R., Gilliland, A., and Dennis, R.: Environmental impact of atmospheric NH_3 emissions under

488   present and future conditions in the eastern United States, Geophys. Res. Lett., 35, 28,

489   https://doi.org/10.1029/2008gl033732, 2008.

490 Pye, H. O. T.; Nenes, A.; Alexander, B.; Ault, A. P.; Barth, M. C.; Clegg, S. L.; Collett Jr, J. L.; Fahey,

491   K. M.; Hennigan, C. J.; Herrmann, H.; Kanakidou, m.; Kelly, J. T.; Ku, L.; McNeill, V. F.; Riemer,

492   N.; Schaefer, T.; Shi, G.; Tilgner, A.; Walker, J.T.; Wang, T.; Weber, R.; Xing, J.; Zaveri, R. A.;

493   Zuend, A. The acidity of atmospheric particles and clouds. Atmos. Chem. Phys., 20, 4809–4888,

494   https://doi.org/10.5194/acp-20-4809-2020, 2020.

495 Rengarajan, R., Sudheer, A. K., and Sarin, M. M.: Aerosol acidity and secondary organic aerosol

496   formation during wintertime over urban environment in western India, Atmos. Environ., 45,

497   1940–1945, https://doi.org/10.1016/j.atmosenv.2011.01.026, 2011.

498 Seinfeld, J. H., Pandis, S. N., and Noone, K. J.: Atmospheric chemistry and physics: From air pollution

499   to climate change, Phys. Today., 51, 88–90, https://doi.org/10.1063/1.882420, 1998.

500 Sharma, B., Jia, S., Polana, A. J., Ahmed, M. S., Haque, R. R., Singh, S., Mao, J., and Sarkar, S.:

501   Seasonal variations in aerosol acidity and its driving factors in the eastern Indo-Gangetic Plain:

502   A quantitative analysis, Chemosphere., 305, 135490,

503   https://doi.org/10.1016/j.chemosphere.2022.135490, 2022.

504 Shi, G., Xu, J., Peng, X., Xiao, Z., Chen, K., Tian, Y., Guan, X., Feng, Y., Yu, H., Nenes, A., and Russell,

505   A. G.: pH of aerosols in a polluted atmosphere: source contributions to highly acidic aerosol,

506   Environ. Sci. Technol., 51, 4289–4296, https://doi.org/10.1021/acs.est.6b05736, 2017.

507 Shi, X., Nenes, A., Xiao, Z., Song, S., Yu, H., Shi, G., Zhao, Q., Chen, K., Feng, Y., and Russell, A.

508   G.: High-resolution data sets unravel the effects of sources and meteorological conditions on

509   nitrate and its gas-particle partitioning, Environ. Sci. Technol., 53, 3048–3057,

510   https://doi.org/10.1021/acs.est.8b06524, 2019.

511 Song, S., Nenes, A., Gao, M., Zhang, Y., Liu, P., Shao, J., Ye, D., Xu, W., Lei, L., Sun, Y., Liu, B.,

512   Wang, S., and McElroy, M. B.: Thermodynamic modeling suggests declines in water uptake and

513   acidity of inorganic aerosols in Beijing winter haze events during 2014/2015–2018/2019, Environ.

514   Sci. Technol. Lett., 6, 752–760, https://doi.org/10.1021/acs.estlett.9b00621, 2019.

515 Su, H., Cheng, Y., and Pöschl, U.: New Multiphase Chemical Processes Influencing Atmospheric

516   Aerosols, Air Quality, and Climate in the Anthropocene, Acc. Chem. Res., 53, 2034–2043,

517   https://doi.org/10.1021/acs.accounts.0c00246, 2020.

518 Surratt, J. D., Chan, A. W. H., Eddingsaas, N. C., Chan, M., Loza, C. L., Kwan, A. J., Hersey, S. P.,

519   Flagan, R. C., Wennberg, P. O., and Seinfeld, J. H.: Reactive intermediates revealed in

520   secondary organic aerosol formation from isoprene, Proc. Natl. Acad. Sci., 107, 6640–6645,

521   https://doi.org/10.1073/pnas.0911114107, 2010.

522 Tao, Y. and Murphy, J. G.: The sensitivity of $PM_{2.5}$ acidity to meteorological parameters and chemical

composition changes: 10-year records from six Canadian monitoring sites, Atmos. Chem. Phys., 19, 9309–9320, https://doi.org/10.5194/acp-19-9309-2019, 2019.

Tian, Y.; Chen, G.; Wang, H.; Huang-Fu, Y.; Shi, G.; Han, B.; and Feng, Y.: Source regional contributions to $PM_{2.5}$ in a megacity in China using an advanced source regional apportionment method. Chemosphere., 147, 256–263, https://doi.org/10.1016/j.chemosphere.2015.12.132, 2016.

Tremper, A.; Font, A.; Priestman, M.; Hamad, S.; Chung, T.; Pribadi, A.; Brown, R.; Goddard, S.; Grassineau, N.; Petterson, K.; Kelly, F.; Green, D.: Field and laboratory evaluation of a high time resolution x-ray fluorescence instrument for determining the elemental composition of ambient aerosols, Atmos. Meas. Tech., 11, 3541–3557, https://doi.org/10.5194/amt-11-3541-2018, 2018.

Wang, C., Yin, S., Bai, L., Zhang, X., Gu, X., Zhang, H., Lu, Q., and Zhang, R.: High-resolution ammonia emission inventories with comprehensive analysis and evaluation in Henan, China, 2006–2016, Atmos. Environ., 193, 11–23, https://doi.org/10.1016/j.atmosenv.2018.08.063, 2018.

Wang, G., Chen, J., Xu, J., Yun, L., Zhang, M., Li, H., Qin, X., Deng, C., Zheng, H., Gui, H., Liu, J., and Huang, K.: Atmospheric processing at the Sea-Land interface over the South China Sea: Secondary aerosol formation, aerosol acidity, and role of sea salts, J. Geophys. Res. Atmos., 127, https://doi.org/10.1029/2021jd036255, 2022.

Wang, J.; Gao, J.; Che, F.; Wang, Y.; Lin, P.; Zhang, Y.: Dramatic changes in aerosol composition during the 2016–2020 heating seasons in Beijing–Tianjin–Hebei region and its surrounding areas: The role of primary pollutants and secondary aerosol formation, Sci. Total Environ., 849, 157621, https://doi.org/10.1016/j.scitotenv.2022.157621, 2022.

Wang, L., Du, H., Chen, J., Zhang, M., Huang, X., Tan, H., Kong, L., and Geng, F.: Consecutive transport of anthropogenic air masses and dust storm plume: Two case events at Shanghai, China, Atmos. Res., 127, 22–33, https://doi.org/10.1016/j.atmosres.2013.02.011, 2013.

Wang, S., Yin, S., Zhang, R., Yang, L., Zhao, Q., Zhang, L., Yan, Q., Jiang, N., and Tang, X.: Insight into the formation of secondary inorganic aerosol based on high-time-resolution data during haze episodes and snowfall periods in Zhengzhou, China, Sci. Total Environ., 660, 47–56, https://doi.org/10.1016/j.scitotenv.2018.12.465, 2019.

Wang, S.; Wang, L.; Li, Y.; Wang, C.; Wang, W.; Yin, S.; Zhang, R.; Effect of ammonia on fine-particle pH in agricultural regions of China: comparison between urban and rural sites, Atmos. Chem. Phys., 20, 2719–2734, https://doi.org/10.5194/acp-20-2719-2020, 2020.

Wang, Y. Q., Zhang, X. Y., and Draxler, R. R.: TrajStat: GIS-based software that uses various trajectory statistical analysis methods to identify potential sources from long-term air pollution measurement data, Environ. Model. Softw., 24, 938–939, https://doi.org/10.1016/j.envsoft.2009.01.004, 2009.

Wang, Z., Pan, X., Uno, I., Chen, X., Yamamoto, S., Zheng, H., Li, J., and Wang, Z.: Importance of mineral dust and anthropogenic pollutants mixing during a long–lasting high PM event over East Asia, Environ. Pollut., 234, 368–378, https://doi.org/10.1016/j.envpol.2017.11.068, 2018.

Weber, R.; Guo, H.; Russell, A.; Nenes, A.: High aerosol acidity despite declining atmospheric sulfate concentrations over the past 15 years, Nature Geoscience., 9, 282–285, https://doi.org/10.1038/ngeo2665, 2016.

Wei, Y.; Wang, S.; Jiang, N.; Zhang, R.; and Hao, Q. Comparative multi-model study of $PM_{2.5}$ acidity trend changes in ammonia-rich regions in winter: Based on a new ammonia concentration assessment method, J. Hazard., 458, 15, https://doi.org/10.1016/10.1016/j.jhazmat.2023.131970, 2023.

Wen, L., Xue, L., Wang, X., Xu, C., Chen, T., Yang, L., Wang, T., Zhang, Q., and Wang, W.: Summertime fine particulate nitrate pollution in the North China Plain: increasing trends, formation mechanisms and implications for control policy, Atmos. Chem. Phys., 18, 11261–11275, https://doi.org/10.5194/acp-18-11261-2018, 2018.

Wexler, A. S. and Seinfeld, J. H.: Second-generation inorganic aerosol model, Atmos. Environ., Part A. General Topics, 25, 2731-2748, https://doi.org/10.1016/0960-1686(91)90203-J, 1991.

Xie, Y., Wang, G., Wang, X., Chen, J., Chen, Y., Tang, G., Wang, L., Ge, S., Xue, G., Wang, Y., and Gao, J.: Nitrate-dominated $PM_{2.5}$ and elevation of particle pH observed in urban Beijing during the winter of 2017, Atmos. Chem. Phys., 20, 5019–5033, https://doi.org/10.5194/acp-20-5019-2020, 2020.

Xu, K., Yin, L., Chen, Q., Liao, D., Ji, X., Zhang, K., Wu, Y., Xu, L., Li, M., Fan, X., Zhang, F., Huang, Z., Chen, J., and Hong, Y.: Quantitative analysis of influencing factors to aerosol pH and its responses to $PM_{2.5}$ and O_3 pollution in a coastal city, J. Environ. Sci., 151, 284–297, https://doi.org/10.1016/j.jes.2024.03.044, 2025.

Yu, F., Yan, Q., Jiang, N., Su, F., Zhang, L., Yin, S., Li, Y., Zhang, R., and Chen, L.: Tracking pollutant characteristics during haze events at background site Zhongmu, Henan Province, China, Atmos. Pollut. Res., 8, 64–73, https://doi.org/10.1016/j.apr.2016.07.005, 2017.

Zhai, S.; Jacob, DJ.; Wang, X.; Shen, L.; Li, K.; Zhang, Y.; Gui, K.; Zhao, T.; Liao, H. Fine particulate matter ($PM_{2.5}$) trends in China, 2013–2018: separating contributions from anthropogenic emissions and meteorology, Atmos. Chem. Phys., 19, 11031–11041, https://doi.org/10.5194/acp-19-11031-2019, 2019.

Zhang, B., Shen, H., Liu, P., Guo, H., Hu, Y., Chen, Y., Xie, S., Xi, Z., Skipper, T. N., and Russell, A. G.: Significant contrasts in aerosol acidity between China and the United States, Atmos. Chem. Phys., 21, 8341–8356, https://doi.org/10.5194/acp-21-8341-2021, 2021.

Zhang, G., Ding, C., Jiang, X., Pan, G., Wei, X., and Sun, Y.: Chemical compositions and sources contribution of atmospheric particles at a typical steel industrial urban site, Sci. Rep., 10, 7654, https://doi.org/10.1038/s41598-020-64519-x, 2020.

Zhang, Z., Dong, Z., Zhang, C., Qian, G., and Lei, C.: The geochemical characteristics of dust material and dust sources identification in northwestern China, J. Geochem. Explor., 175, 148–155, https://doi.org/10.1016/j.gexplo.2016.11.006, 2017.

Zhang, Z., Kuang, Z., Yu, C., Wu, D., Shi, Q., Zhang, S., Wang, Z., and Liu, D.: Trans–boundary dust transport of dust storms in Northern China: A study utilizing ground–based lidar network and CALIPSO satellite, Remote sens.,16, 1196, https://doi.org/10.3390/rs16071196, 2024.

Zheng, G., Su, H., and Cheng, Y.: Revisiting the key driving processes of the decadal trend of aerosol acidity in the U.S, Acs. Environ. Au., 2, 346–353, https://doi.org/10.1021/acsenvironau.1c00055, 2022.

Zheng, G., Su, H., Wang, S., Andreae, M. O., Pöschl, U., and Cheng, Y.: Multiphase buffer theory

604 explains contrasts in atmospheric aerosol acidity, Science., 369, 1374–1377,
605   https://doi.org/10.1126/science.aba3719, 2020.

606 Zhou, M., Zheng, G., Wang, H., Qiao, L., Zhu, S., Huang, D., An, J., Lou, S., Tao, S., Wang, Q., Yan,
607   R., Ma, Y., Chen, C., Cheng, Y., Su, H., and Huang, C.: Long-term trends and drivers of aerosol
608   pH in eastern China, Atmos. Chem. Phys., 22, 13833–13844, https://doi.org/10.5194/acp-22-
609   13833-2022, 2022.

610 Zhou, W., Gao, M., He, Y., Wang, Q., Xie, C., Xu, W., Zhao, J., Du, W., Qiu, Y., Lei, L., Fu, P., Wang,
611   Z., Worsnop, D. R., Zhang, Q., and Sun, Y.: Response of aerosol chemistry to clean air action in
612   Beijing, China: Insights from two-year ACSM measurements and model simulations, Environ
613   Pollut., 255, 113345, https://doi.org/10.1016/j.envpol.2019.113345, 2019.

614 Zuend, A. and Seinfeld, J. H.: Modeling the gas-particle partitioning of secondary organic aerosol: the
615   importance of liquid-liquid phase separation, Atmos. Chem. Phys., 12, 3857–3882,
616   https://doi.org/10.5194/acp-12-3857-2012, 2012.

617 Zuend, A., Marcolli, C., Peter, T., and Seinfeld, J. H.: Computation of liquid-liquid equilibria and phase
618   stabilities: implications for RH-dependent gas/particle partitioning of organic-inorganic aerosols,
619   Atmos. Chem. Phys., 10, 7795–7820, https://doi.org/10.5194/acp-10-7795-2010, 2010.

620
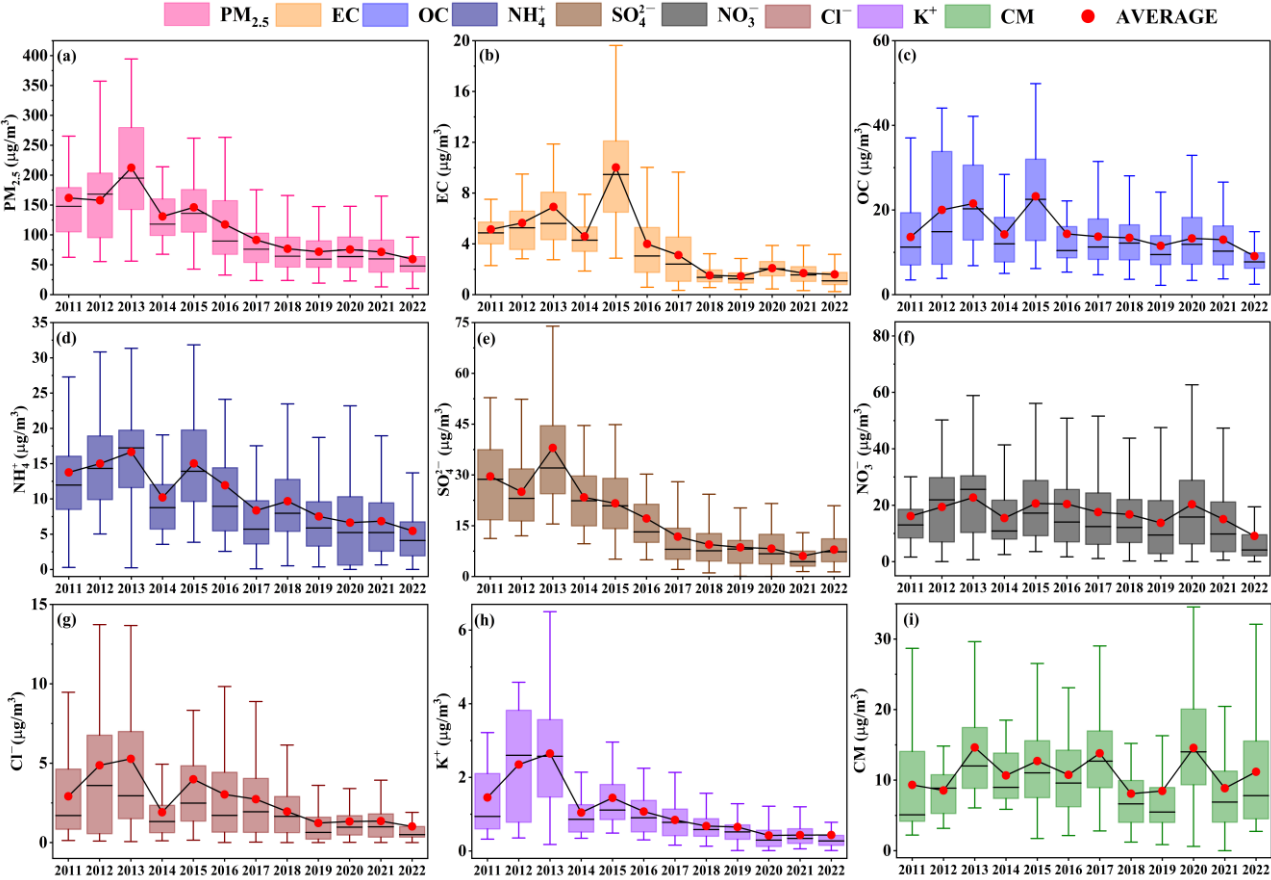
Figures

623 Figure 1. Long-term trends in the concentrations of PM$_{2.5}$ and its chemical components in from 2011
624 to 2022 in Zhengzhou. Box plots depict annual averages (red dots) and medians (black lines), the
625 top, middle, and bottom lines represent the 75, 50, and 25 percentiles of statistical data, respectively,
626 and the upper and lower whiskers represent the 90 and 10 percentiles of statistical data, respectively.
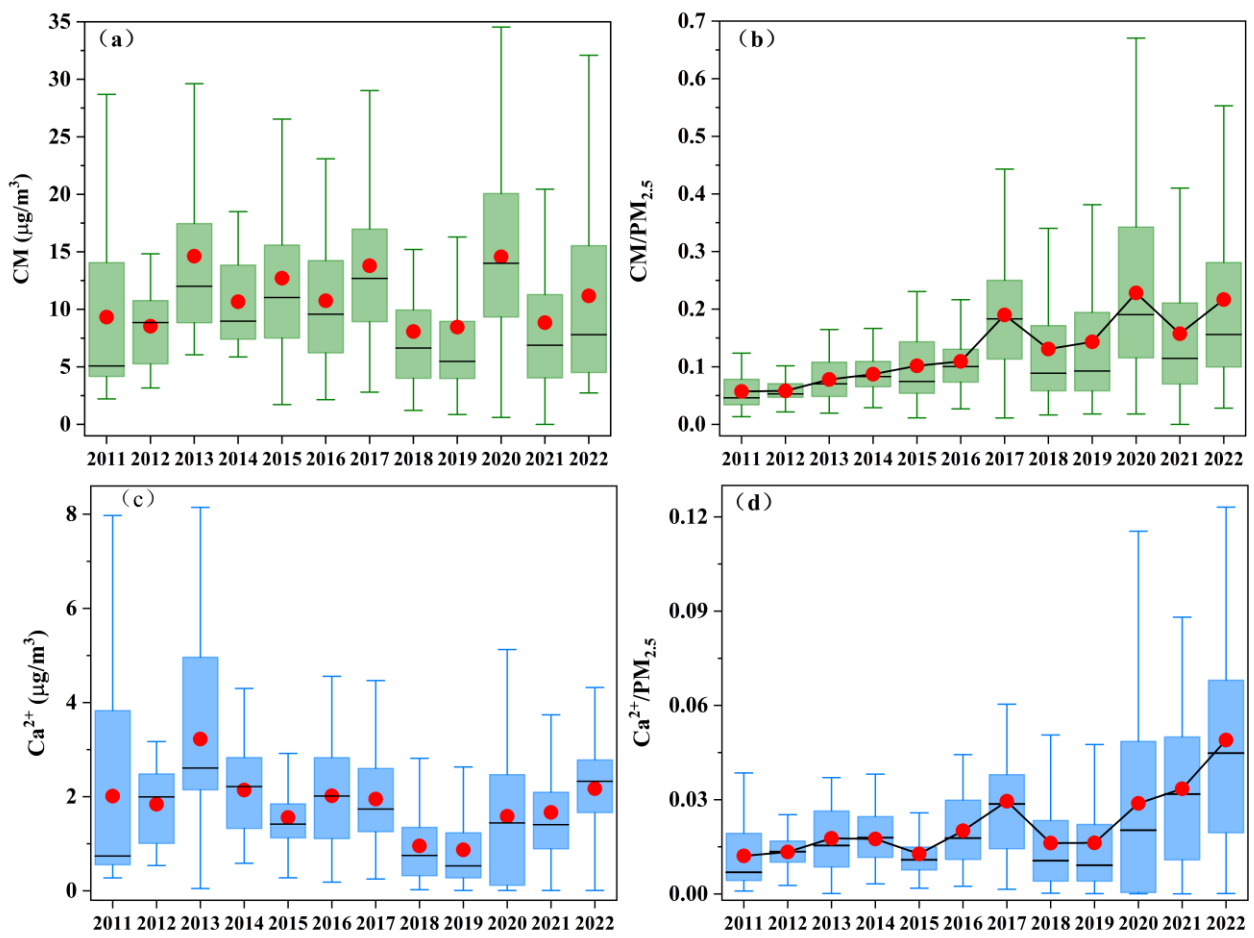
Figure 2. (a) and (c) Long-term trends in CM and Ca^{2+} concentrations in Zhengzhou from 2011 to 2022, respectively. Box plots depict annual averages (red dots) and medians (black lines). (b) and (d) Long-term trends in the proportions of CM and Ca^{2+} in $PM_{2.5}$, respectively.

631
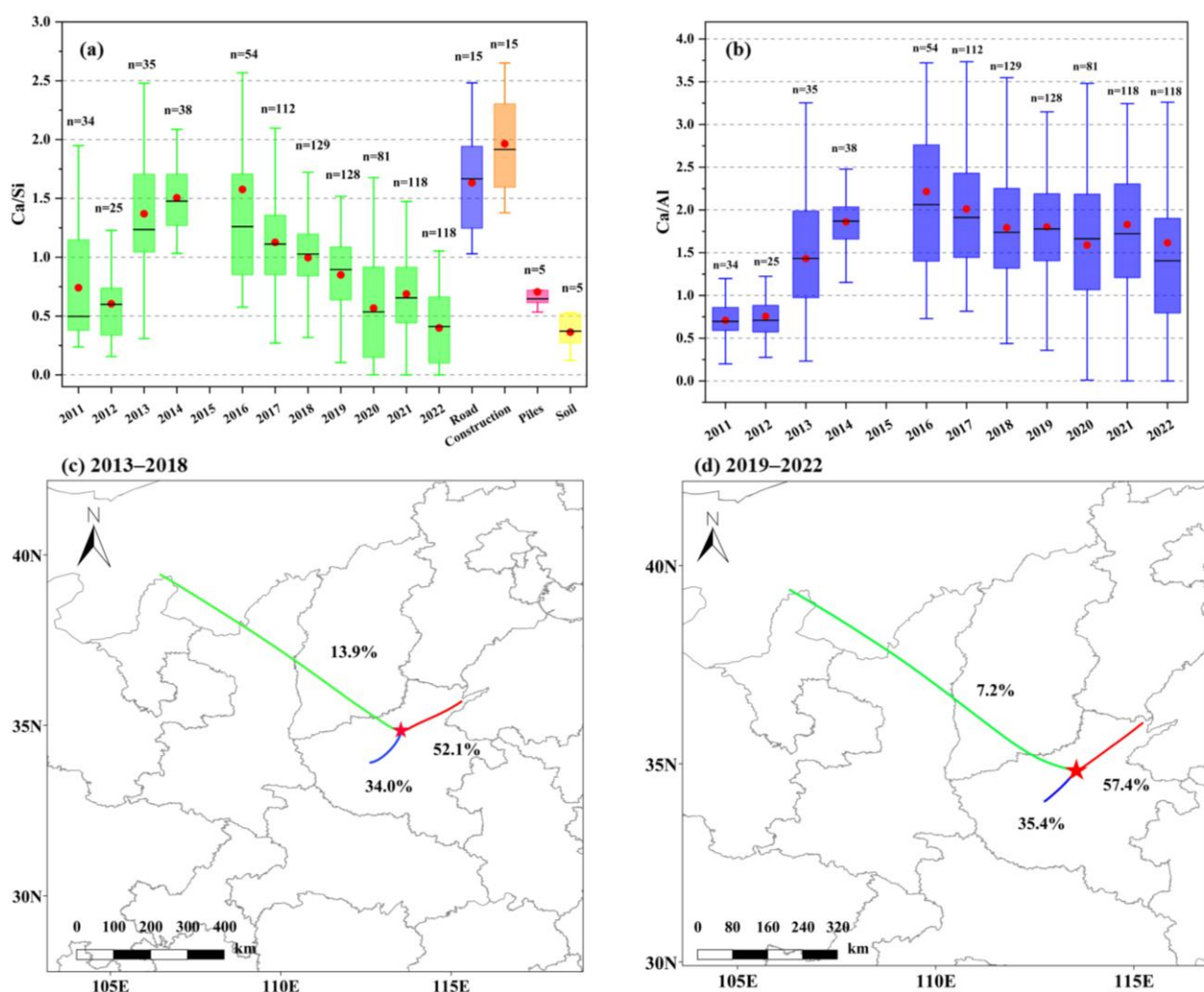
Figure 3. (a) The annual Ca/Si ratios in Zhengzhou from 2011 to 2022 compared with those in various dust sources (specific values and references in Table S7). The red dots and black lines in the box plots represent the annual averages and medians, respectively, with n indicating the sample size. (b) The Ca/Al ratios in Zhengzhou from 2011 to 2022. The red dots and black lines in the box plots represent the annual averages and medians, respectively, with n indicating the sample size. (c) and (d) The transport pathways of CM during 2013–2018 and 2019–2022, respectively.

638
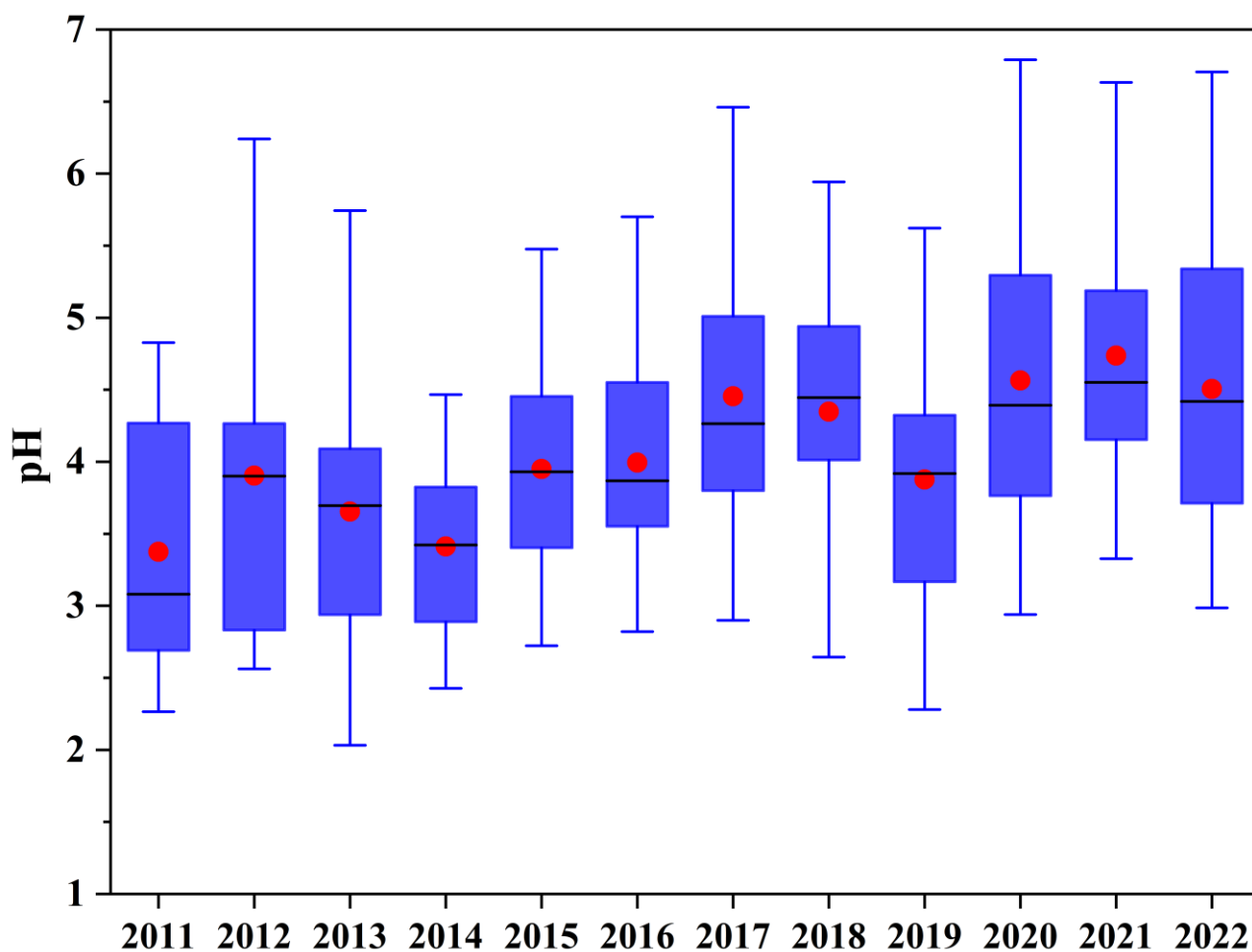
Figure 4. The time series of particle pH in Zhengzhou from 2011 to 2022. In the boxplots, red dots
and black lines represent the annual mean and median values, respectively.

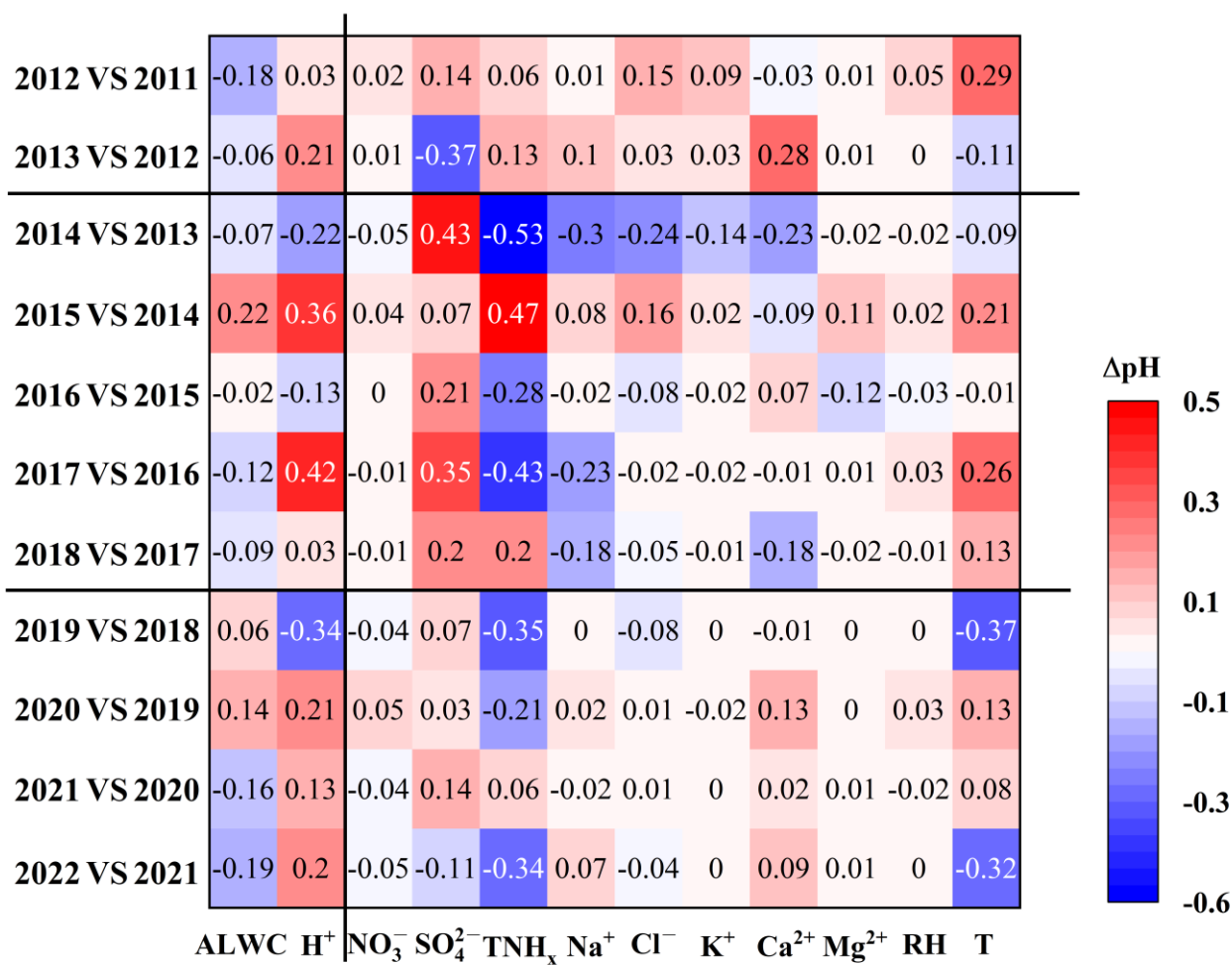|	ALWC	H^+	NO_3^-	SO_4^{2-}	TNH_x	Na^+	Cl^-	K^+	Ca^{2+}	Mg^{2+}	RH	T
2012 VS 2011	-0.18	0.03	0.02	0.14	0.06	0.01	0.15	0.09	-0.03	0.01	0.05	0.29
2013 VS 2012	-0.06	0.21	0.01	-0.37	0.13	0.1	0.03	0.03	0.28	0.01	0	-0.11
2014 VS 2013	-0.07	-0.22	-0.05	0.43	-0.53	-0.3	-0.24	-0.14	-0.23	-0.02	-0.02	-0.09
2015 VS 2014	0.22	0.36	0.04	0.07	0.47	0.08	0.16	0.02	-0.09	0.11	0.02	0.21
2016 VS 2015	-0.02	-0.13	0	0.21	-0.28	-0.02	-0.08	-0.02	0.07	-0.12	-0.03	-0.01
2017 VS 2016	-0.12	0.42	-0.01	0.35	-0.43	-0.23	-0.02	-0.02	-0.01	0.01	0.03	0.26
2018 VS 2017	-0.09	0.03	-0.01	0.2	0.2	-0.18	-0.05	-0.01	-0.18	-0.02	-0.01	0.13
2019 VS 2018	0.06	-0.34	-0.04	0.07	-0.35	0	-0.08	0	-0.01	0	0	-0.37
2020 VS 2019	0.14	0.21	0.05	0.03	-0.21	0.02	0.01	-0.02	0.13	0	0.03	0.13
2021 VS 2020	-0.16	0.13	-0.04	0.14	0.06	-0.02	0.01	0	0.02	0.01	-0.02	0.08
2022 VS 2021	-0.19	0.2	-0.05	-0.11	-0.34	0.07	-0.04	0	0.09	0.01	0	-0.32

Figure 5. Contribution of each component to the changes in pH (ΔpH) between adjacent years. The difference between component concentrations and meteorological parameters between adjacent years is listed in Table S8.

645 **Table**

646 Table 1. Annual average concentrations of PM$_{2.5}$ and its components from 2011 to 2022 in Zhengzhou,
647 China (μg/m^3).

Years	PM$_{2.5}$	EC	OC	NO$_3^-$	SO$_4^{2-}$	NH$_4^+$	CM	Ca^{2+}
2011	161.9±81.4	5.1±2.1	13.6±8.6	16.2±11.2	29.6±14.3	13.8±8.3	9.3±7.3	2.0±2.2
2012	157.9±71.2	5.6±2.5	20.0±13.4	20.2±13.7	25.0±11.2	15.0±7.1	8.5±3.4	1.8±0.8
2013	212.4±101.5	6.9±3.8	21.5±10.4	22.7±13.2	38.0±19.9	17.1±6.9	14.6±8.3	3.2±2.1
2014	130.8±48.7	4.6±2.0	14.2±8.2	15.5±10.8	23.4±9.3	10.2±6.2	10.7±4.4	2.1±1.0
2015	146.1±61.0	10.0±4.7	23.2±11.6	20.6±14.5	21.6±9.8	15.7±7.5	12.7±6.8	1.6±0.7
2016	117.4±73.5	4.0±2.8	14.4±10.0	20.4±18.7	17.1±11.3	11.9±10.6	10.8±5.3	2.0±1.1
2017	91.5±61.1	3.1±2.5	13.7±7.5	17.6±15.9	11.8±11.6	8.4±7.9	13.8±6.5	2.0±1.0
2018	76.8±41.6	1.5±0.7	13.4±7.3	16.7±13.5	9.4±6.0	9.7±6.1	8.1±5.7	1.0±0.8
2019	68.4±34.8	1.5±0.8	11.5±6.8	13.8±13.9	8.6±6.4	7.5±6.1	8.5±7.8	0.9±0.9
2020	75.5±31.8	2.1±0.9	13.3±7.9	18.6±14.2	8.3±5.6	6.7±6.6	14.6±7.6	1.6±1.4
2021	71.5±45.9	1.7±0.9	13.0±8.0	15.1±15.1	6.1±4.5	6.8±6.0	8.9±7.0	1.7±1.2
2022	59.5±41.1	1.6±1.5	9.1±8.1	10.0±14.4	7.9±4.5	5.5±5.4	11.2±8.3	2.2±1.1

648

649